Electron Screening and Kinetic-Energy Oscillations in a Strongly Coupled Plasma

Y. C. Chen, C. E. Simien, S. Laha, P. Gupta, Y. N. Martinez, P. G. Mickelson, S. B. Nagel, and T. C. Killian

Department of Physics and Astronomy, Rice University, Houston, Texas 77005, USA
and Rice Quantum Institute, Rice University, Houston, Texas 77005, USA

We study equilibration of strongly coupled ions in an ultracold neutral plasma produced by photo-ionizing laser-cooled and trapped atoms. By varying the electron temperature, we show that electron screening modifies the equilibrium ion temperature. Even with few electrons in a Debye sphere, the screening is well described by a model using a Yukawa ion-ion potential. We also observe damped oscillations of the ion kinetic energy that are a unique feature of equilibration of a strongly coupled plasma.

A plasma becomes strongly coupled when the electrical interaction energy between the charged particles exceeds the thermal energy. Strong coupling is observed in dense astrophysical environments [1], such as the interiors of gas giant planets, and in laser-cooled ions [2], dusty plasmas [3], and solid targets [4] and clusters [5] irradiated by pulsed high-intensity lasers. Equilibration in these systems is of particular interest because it involves the establishment of spatial correlations between particles.

There has been significant theoretical study of the equilibration of strongly coupled plasmas [6–12], especially in the context of plasmas produced with high-intensity lasers. In addition to generating fundamental interest, this problem challenges computational resources and techniques. Experimental results have been lacking, however, because of the fast time scales involved and limited diagnostics.

Ultracold neutral plasmas [13], produced by photoionizing clouds of laser-cooled and trapped atoms, are ideal for experimental studies. The equilibration of the plasma is relatively slow (~ 100 ns) due to lower plasma density. Ultracold neutral plasmas also offer a high level of control and diagnostics. By varying laser intensities and wavelengths, it is possible to accurately set the initial density and energy of the system. Optical imaging [14] provides an *in situ* probe of plasma properties with excellent spatial, temporal, and spectral resolution.

In this Letter, we explore ion equilibration during the first microsecond after the plasma is created. The density sets the time and the energy scale for equilibration, but electron screening effects are evident. Even when the number of electrons per Debye sphere is small, the equilibration temperature of the ions agrees with a model [15] that uses a Yukawa ion-ion potential.

We also observed oscillations of the ion kinetic energy. For many years, this phenomenon has been the subject of intense study through analytic calculations [7] and simulations [6,8–12] of one-component strongly coupled plasmas, but it has not previously been observed experimentally. The oscillations and their damping reflect universal dynamics of a Coulomb system with spatial correlations.

Details on laser cooling, plasma formation, and imaging are given in [14,16]. The experiment starts with strontium atoms that are cooled and trapped in a magneto-optical trap (MOT). The neutral atom cloud is characterized by a temperature of about 10 mK, 2×10^8 atoms, and a Gaussian density distribution. We vary the atom density by changing the MOT parameters, or by turning the MOT off and releasing the atoms in a ballistic expansion. Up to 30% of the neutral atoms are then ionized with one photon from the cooling laser and one photon from a pulsed dye laser. The ion density distribution equals the atom distribution at the time of photoionization and is given by $n_i(r) = n_{0i} \exp(-r^2/2\sigma^2)$, with σ from 0.6 to 1 mm and n_{0i} from 2×10^9 to 1.4×10^{10} cm^{-3}. The electron density, $n_e(\mathbf{r})$, closely follows the ion density, and the initial electron temperature is given by $T_e = 2E_e/3k_B$, where E_e is the detuning of the pulsed laser above the ionization threshold.

At an adjustable delay time (t_{delay}) after photoionization, a collimated laser beam, tuned near resonance with the Sr$^+$ $^2S_{1/2} - {}^2P_{1/2}$ transition at 422 nm, illuminates the plasma and falls on an intensified charge coupled device camera. By varying t_{delay}, we study the evolution of the plasma after formation.

The optical depth (OD) for a laser propagating along the z axis is defined by $\text{OD}(x, y) = \log[I_{\text{background}}(x, y)/I_{\text{image}}(x, y)]$, where $I_{\text{background}}$ and I_{image} are laser intensities without and with the plasma present. By integrating the optical depth over x and y for images taken at different image beam frequencies, ν, we obtain the absorption spectrum

$$S(\nu) = \int dx dy \, \text{OD}(x, y) = \int d^3 r \, n_i(r) \alpha[\nu, T_i(r)]$$
$$\equiv N_i \alpha(\nu, T_{i,\text{eff}}). \tag{1}$$

We have used Beer's law to relate $S(\nu)$ to the absorption cross section, $\alpha[\nu, T_i(r)]$, and the ion density. The absorption cross section is a function of temperature due to the Doppler broadening, and since we expect the temperature to vary with density, we allow α to vary with position. The

absorption cross section has a Voigt profile resulting from
the convolution of the Gaussian Doppler broadening with
a Lorentzian with width $\gamma = \gamma_0 + \gamma_{\text{laser}}$. Here, $\gamma_0 =$
22 MHz is the natural width of the transition, and $\gamma_{\text{laser}} =$
(5 ± 2) MHz is the measured linewidth of the laser. As
shown in the second line of Eq. (1), we fit the spectrum to a
single Voigt profile with effective temperature $T_{i,\text{eff}}$. N_i is
the number of ions. We will discuss below how $T_{i,\text{eff}}$ relates
to the average ion temperature in the plasma.

Figure 1(a) shows the evolution of $T_{i,\text{eff}}$ for three differ-
ent densities. The rapid increase in the temperature for
$t_{\text{delay}} < 300$ ns is due to disorder-induced heating. This
originates from conversion of Coluomb potential energy
into kinetic energy as the ions evolve from a completely
disordered state to one with some degree of spatial corre-
lations. This was predicted in [15] and observed in numeri-
cal simulations [12,17,18] and the first experimental
studies with optical imaging [14].

The time scale of the heating is the inverse ion plasma
frequency $\omega_{pi}^{-1} = \sqrt{m_i \varepsilon_0 / n_i e^2} \approx 100$ ns. The energy scale
is $T_C = e^2 / 4\pi\varepsilon_0 a k_B \approx 5$ K, where $a = (4\pi n_i/3)^{-1/3}$ is
the Wigner-Seitz radius. Figure 1(b) shows data with time
scaled by the average inverse plasma frequency and tem-
perature scaled by T_C. The three curves coincide very well
in the time axis, but show slight deviation in the tempera-
ture axis. The deviation indicates the effects of electron
screening of the ion-ion interaction.

A detailed expression for the equilibrium ion tempera-
ture, including screening effects, was derived in [15].
Assuming complete disorder and stationary ions at $t_{\text{delay}} =$
0, and incorporating electron screening through a Yukawa
ion-ion potential [19,20],

$$T_i = \frac{2}{3} \frac{e^2}{4\pi\varepsilon_0 a k_B} \mid \tilde{U} + \kappa/2 \mid . \qquad (2)$$

Here, $\kappa = a/\lambda_D$, where $\lambda_D = (\varepsilon_0 k_B T_e / n_i e^2)^{1/2}$ is the
Debye length. The quantity $\tilde{U} \equiv U/(N_i e^2 / 4\pi\varepsilon_0 a)$ is the
potential energy per particle in units of $e^2/4\pi\varepsilon_0 a$, and it
has been tabulated in [19]. Equation (2) is complicated by
the fact that $\tilde{U}$ is a function of n_i and T_i. From the table of

$\tilde{U}$ and using an iterative numerical routine, T_i can be
obtained for a given n_i and T_e.

The effects of electron screening are quantified by the
factor $\mid \tilde{U} + \kappa/2 \mid$. Colder electron temperature and
higher density lead to a smaller Debye length and greater
screening of the ion-ion potential. This decreases the po-
tential energy in the initial system, and thus, compared to a
system in which there is no screening, decreases the equili-
bration temperature reached. This effect is evident in
Fig. 2, which shows data from three different initial elec-
tron energies but the same ion density distribution. To
quantitatively compare the data in Figs. 1 and 2 with
Eq. (2) we must account for two factors. The first is the
effect of the inhomogeneous density distribution. We ex-
pect the ion temperature to vary with density because
global thermal equilibrium occurs on a hydrodynamic
time scale, σ/v, which is on the order of tens of μs, where
v is the ion acoustic wave velocity. Local thermal equili-
bration occurs on a much faster time scale, $\sim\omega_{pi}^{-1}$ [21]. If
we assume a temperature distribution given by Eq. (2),
numerical simulations [22] show that $T_{i,\text{eff}} = (0.95 \pm$
$0.05)T_{i,\text{av}}$. Here $T_{i,\text{av}}$ is the average ion temperature found
by averaging Eq. (2) over the density profile.

To extract the average ion temperature, we must also
account for acceleration of the ions by the electron pres-
sure. This was studied experimentally in [14,23] and theo-
retically in [24,25], and it is evident in the continuing
increase in $T_{i,\text{eff}}$ in Figs. 1 and 2 for $t_{\text{delay}} > 500$ ns. This
acceleration will lead to expansion of the plasma after a
time on the order of 10 μs, and although it is not a heating
effect, it contributes to the Doppler width of the spectrum.
Numerical analysis [22], assuming a temperature distribu-
tion given by Eq. (2), shows that the effect of plasma
expansion on the effective ion temperature can be approxi-
mated by

$$T_{i,\text{eff}}(t_{\text{delay}}) = CT_{i,\text{av}}[1 + 1/C(t_{\text{delay}}/t_{\text{exp}})^2], \qquad (3)$$
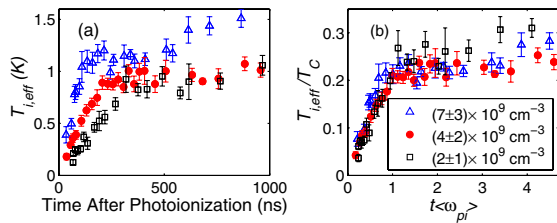

FIG. 1 (color online). The effective ion temperature, $T_{i,\text{eff}}$,
versus time after photoionization for an initial electron tempera-
ture of $T_e = 2E_e/3k_B = 38 \pm 6$ K and various plasma densities.
(a) The data are plotted on absolute temperature and time scales.
(b) The time is scaled by the inverse of the average plasma
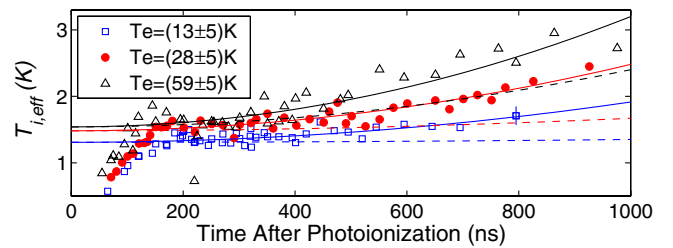period, and $T_{i,\text{eff}}$ is scaled by T_C.

FIG. 2 (color online). Effective ion temperature versus time
after photoionization for various electron temperatures. The peak
ion density for all data is $n_{0i} = (1.4 \pm 0.5) \times 10^{10}$ cm^{-3}. The
solid curves are fits of the data based on Eq. (3). The fit
determines the equilibrium $T_{i,\text{av}}$ and T_e. The fit T_e, (82 ± 5),
(64 ± 6), and (45 ± 6) K are higher than the expected initial T_e
shown in the legend, indicating electron heating. The dashed
curves show the increase in $T_{i,\text{eff}}$ due to radial acceleration
expected for $T_e = 2E_e/3k_B$. A typical data error bar is shown.

where $C = (0.95 \pm 0.05)$ is a constant and t_{exp} is the time scale when the Doppler broadening contributed by plasma expansion is comparable to the thermal Doppler broadening. It is given by

$$t_{exp} = \sigma\sqrt{m_i/k_B T_e}\sqrt{T_{i,av}/T_e}. \qquad (4)$$

Because we want to check the accuracy of Eq. (2), and we assume this equation in our analysis, strictly speaking, our strongest conclusion can be that our data are consistent with Eq. (2). However, we found [22] that Eq. (3) is accurate for a range of temperature distributions, from global thermal equilibrium to local thermal equilibrium at a temperature expected in the absence of electron screening. It can be shown analytically that Eq. (3) has the correct long-time limit for when the plasma reaches global equilibrium, or when the expansion velocity greatly exceeds the thermal velocity. We do not believe our analysis is very sensitive to a particular assumption of $T_i(r)$.

In Fig. 2, using Eq. (3), we extract $T_{i,av}$ and T_e from the data. The model addresses the dynamics after local equilibration, not the disorder-induced heating phase during the first 100 ns. The fit T_e exceed $2E_e/3k_b$ for the data shown. As predicted by theory [17,18,24,26], this effect becomes larger as the initial Coulomb coupling parameter for the electrons, $\Gamma_e = \kappa^3/3 = e^2/(4\pi\varepsilon_0 a k_B T_e)$, approaches unity. ($\Gamma_e = 0.5$ for the coldest electron temperature data in Fig. 2, assuming $T_e = 2E_e/3k_B$ and using the peak density.) Likely mechanisms for heating are recombination, continuum lowering, and disorder-induced electron heating. We plan to study this phenomenon in the future, but our main goal now is accurate determination of $T_{i,av}$.

The inferred value of $T_{i,av}$, which is the average ion temperature after the plasma reaches local thermal equilibrium, is shown in Fig. 3. The uncertainty in $T_{i,av}$, of about 0.2 K, is determined by the statistical noise in the data and the uncertainty in C. We also show the theoretical value of $T_{i,av}$, found by averaging Eq. (2) over the density distribution. Uncertainty in this quantity results from unce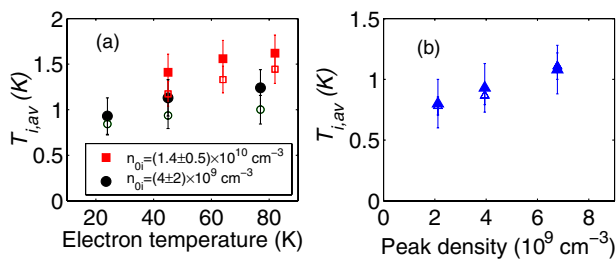rtainty in the value of the peak density. Experimental and theoretical results agree well. It is not initially surprising that Eq. (2) accurately predicts the ion temperature for equilibrating ultracold neutral plasmas. The theory basically expresses energy conservation, as emphasized in [12]. However, for the data in Fig. 3 with the lowest fit T_e and highest n_{0i}, the peak value of κ in the plasma is 0.7. This corresponds to three electrons per Debye sphere ($\kappa^{-3} = n_e 4\pi\lambda_D^3/3$). One might not necessarily expect Eq. (2) to be accurate in this regime because it assumes a Yukawa potential for ion-ion interactions. The Yukawa potential is based on Debye screening and is normally derived for $\kappa^{-3} \gg 1$.

From the measured $T_{i,av}$, T_e, and density distribution, we calculate the average Coulomb coupling constant for Debye-screen ions, $\Gamma_{i,av}^* = \langle \exp[-\kappa(r)]e^2/[4\pi\varepsilon_0 a(r) k_B T_{i,av}]\rangle$. For all the data shown in Fig. 3, $\Gamma_{i,av}^*$ is in the range of 1.7 to 2.5. With lower T_e and higher density, $\Gamma_{i,av}^*$ is slightly higher. The surprisingly small variation in $\Gamma_{i,av}^*$ suggests that disorder-induced heating is a natural feedback mechanism that leads to equilibration just barely in the strongly coupled regime.

Close inspection of Figs. 1 and 2 reveals that at the end of the disorder-induced heating phase the ion temperature overshoots its equilibrium value before settling. This phenomenon is more evident in Fig. 4(a), where $T_{i,av}$ is calculated for an inner and outer region of the plasma image ($\rho = \sqrt{x^2 + y^2} < 0.9\sigma$ and $\rho > 1.48\sigma$, respectively). Each selected annular region contains $1/3$ of the ions and probes a region with significantly less variation in density than in the entire plasma. The region with lower density has lower $T_{i,av}$, supporting our hypothesis of local thermal equilibrium, but the oscillation is the most striking observation.

Intuitively, one can explain this phenomenon as an oscillation of each ion in its local potential energy well. A simple calculation implies that the time for an ion to move an interparticle distance, when accelerated from rest by a force of $e^2/(4\pi\varepsilon_0 a^2)$, varies as $\sim\omega_{pi}^{-1}$, and the observed oscillation occurs at $2\omega_{pi}$. As expected from the density dependence of ω_{pi}, the oscillation period is longer

FIG. 3 (color online).   The comparison between the data and the theoretical calculations. In (a), the density is fixed and the initial T_e is varied. Solid symbols are experimental data and open symbols are theoretical calculations. In (b), the initial T_e is fixed (38 ± 6 K), while the density is varied. The T_e for all theoretical calculations are based on the fit T_e.
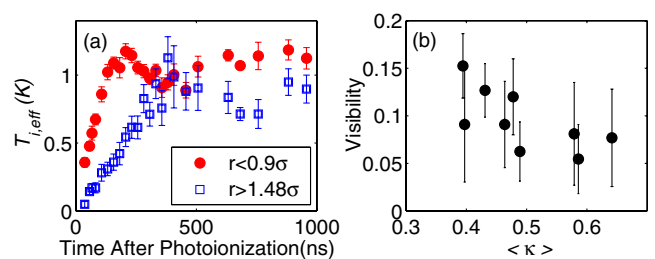

FIG. 4 (color online).   Effective ion temperature obtained from different selected regions of the cloud for $n_{0i} = (4 \pm 2) \times 10^9$ cm^{-3} and initial $T_e = 2E_e/3k_B = 38 \pm 6$ K. In (b), we plot the visibility of the oscillation for the central probed region versus the averaged κ for this region for all our data taken at different conditions.

for the outer region where the average density is lower. This explains why averaging over the entire cloud obscures the oscillation; the motion dephases because of the variation in ω_{pi}. It is questionable whether the ion motion should be called an ion plasma oscillation because there is probably no collective or long range coherence to the motion.

Another way to think of the oscillation is relaxation of the two-particle distribution function in the plasma, which describes two-particle spatial and momentum correlations. Disorder-induced heating and oscillation of the kinetic and the potential energy represent equilibration of spatial correlations. Normally, the time scale for equilibration of the two-particle distribution function is much shorter than the time scale for the one-particle distribution function to reach local thermal equilibrium. This is known as Bogoliubov's hypothesis [27]. For strongly coupled plasmas, however, these time scales both become equal to ω_{pi}^{-1} [9].

Kinetic-energy oscillations at $2\omega_{pi}$ have been observed in molecular dynamics simulations of equilibrating strongly coupled systems [9,11,12]. Calculations [6,28] also show oscillations in the velocity autocorrelation function in equilibrium strongly coupled one-component plasmas. To our knowledge, this is the first experimental observation of the phenomenon.

Numerical results [9] suggest that the damping time for the oscillations is approximately π/ω_{pi} for $\Gamma_i \gtrsim 5$, and that lower Γ_i leads to faster damping. Because our analysis still averages over the z axis of the plasma, which introduces dephasing into the observed oscillations, it is difficult to comment on the damping of the oscillation. But we do find a correlation between the visibility of the oscillation and κ, as shown in Fig. 4(b), suggesting that electron screening plays a role in the damping. The visibility is defined as $(T_{i,\text{eff}}^{\text{peak}} - T_{i,\text{eff}}^{\text{dip}})/(T_{i,\text{eff}}^{\text{peak}} + T_{i,\text{eff}}^{\text{dip}})$, where $T_{i,\text{eff}}^{\text{peak}}$ and $T_{i,\text{eff}}^{\text{dip}}$ are effective ion temperatures at the peak and the dip of the oscillation.

In conclusion, we have studied the equilibration of ultracold neutral plasmas. The screening effect of electrons on the final ion temperature is observed, and experiment and theory agree very well. As predicted from numerical simulations, the ion kinetic energy displays oscillations that are characteristic of equilibrating strongly coupled plasmas.

[1] H. M. V. Horn, Science **252**, 384 (1991).
[2] T. B. Mitchell, J. J. Bollinger, X. P. Huang, W. M. Itano, and D. H. E. Dubin, Phys. Plasmas **6**, 1751 (1999).
[3] J. H. Chu and L. I, Phys. Rev. Lett. **72**, 4009 (1994).
[4] M. Nantel, G. Ma, S. Gu, C. Y. Cote, J. Itatani, and D. Umstadter, Phys. Rev. Lett. **80**, 4442 (1998).
[5] E. Springate, N. Hay, J. W. G. Tisch, M. B. Mason, T. Ditmire, M. H. R. Hutchinson, and J. P. Marangos, Phys. Rev. A **61**, 063201 (2000).
[6] J. P. Hansen, E. L. Pollock, and I. R. McDonald, Phys. Rev. Lett. **32**, 277 (1974).
[7] H. Gould and G. F. Mazenko, Phys. Rev. Lett. **35**, 1455 (1975).
[8] M. Bonitz, D. Semkat, and D. Kremp, Phys. Rev. E **56**, 1246 (1997).
[9] G. Zwicknagel, Contrib. Plasma Phys. **39**, 155 (1999).
[10] K. Morawetz, M. Bonitz, V. G. Morozov, G. Röpke, and D. Kremp, Phys. Rev. E **63**, 020102 (2001).
[11] I. V. Morozov and G. E. Norman, J. Phys. A **36**, 6005 (2003).
[12] T. Pohl, T. Pattard, and J. M. Rost, J. Phys. B **37**, 183 (2004).
[13] T. C. Killian, S. Kulin, S. D. Bergeson, L. A. Orozco, C. Orzel, and S. L. Rolston, Phys. Rev. Lett. **83**, 4776 (1999).
[14] C. E. Simien, Y. C. Chen, P. Gupta, S. Laha, Y. N. Martinez, P. G. Mickelson, S. B. Nagel, and T. C. Killian, Phys. Rev. Lett. **92**, 143001 (2004).
[15] M. S. Murillo, Phys. Rev. Lett. **87**, 115003 (2001).
[16] S. B. Nagel, C. E. Simien, S. Laha, P. Gupta, V. S. Ashoka, and T. C. Killian, Phys. Rev. A **67**, 011401 (2003).
[17] S. G. Kuzmin and T. M. O'Neil, Phys. Plasmas **9**, 3743 (2002).
[18] A. N. Tkachev and S. I. Yakovlenko, Quantum Electron. **30**, 1077 (2000).
[19] S. Hamaguchi, R. T. Farouki, and D. H. E. Dubin, Phys. Rev. E **56**, 4671 (1997).
[20] D. H. E. Dubin and T. M. O'Neil, Rev. Mod. Phys. **71**, 87 (1999).
[21] T. Pohl, T. Pattard, and J. M. Rost, Phys. Rev. A **70**, 033416 (2004).
[22] T. C. Killian, Y. C. Chen, P. Gupta, S. Laha, Y. N. Martinez, P. G. Mickelson, S. B. Nagel, A. D. Saenz, and C. E. Simien, physics/0407138.
[23] S. Kulin, T. C. Killian, S. D. Bergeson, and S. L. Rolston, Phys. Rev. Lett. **85**, 318 (2000).
[24] F. Robicheaux and J. D. Hanson, Phys. Plasmas **10**, 2217 (2003).
[25] T. Pohl, T. Pattard, and J. M. Rost, Phys. Rev. Lett. **92**, 155003 (2004).
[26] S. Mazevet, L. A. Collins, and J. D. Kress, Phys. Rev. Lett. **88**, 55 001 (2002).
[27] D. R. Nicholson, *Introduction to Plasma Theory* (Krieger Publishing Company, Malabar, FL, 1992).
[28] J. P. Hansen, I. R. McDonald, and E. L. Pollock, Phys. Rev. A **11**, 1025 (1975).